https://doi.org/10.5194/acp-2020-1064
Preprint. Discussion started: 3 November 2020

Atmospheric Chemistry and Physics Discussions

Enhancement of nanoparticle formation and growth during the COVID-19 lockdown period in urban Beijing

Xiaojing Shen[1,*], Junying Sun[1], Fangqun Yu[2], Xiaoye Zhang[1], Junting Zhong[1,3], Yangmei Zhang[1], Xinyao Hu[1], Can Xia[1,4], Sinan Zhang[1]

1 State Key Laboratory of Severe Weather & Key Laboratory of Atmospheric Chemistry of CMA, Chinese Academy of Meteorological Sciences, Beijing 100081, China

2 Atmospheric Sciences Research Center, State University of New York at Albany, 251 Fuller Road, Albany, New York 12203, USA

3 University of Chinese Academy of Sciences, Beijing 100049, China

4 Nanjing University of Information Science & Technology, Nanjing 210000, China

Correspondence to: Xiaojing Shen (shenxj@cma.gov.cn)

Abstract. Influenced by the spread of the global 2019 novel coronavirus (COVID-19) pandemic, primary emissions of particles and precursors associated with anthropogenic activities decreased significantly in China during the Chinese New Year of 2020 and the lockdown period (January 24–February 16, 2020), as indicated by approximately 50% reduction of NO_x emission nation-wide based on the open literature. Two-month measurements of the number size distribution of neutral particles and charged ions showed that during the lockdown (LCD) period, the number concentration of particles smaller than 100 nm decreased by approximately 40% compared to the pre-LCD period in January. However, the accumulation mode particles increased by approximately 20% as several polluted episodes contributed to secondary aerosol formation. In this study, new particle formation (NPF) events were found to be enhanced in the nucleation and growth processes during the LCD period, as indicated by higher formation (J_2) and growth rate (*GR*), even as NPF occurrence frequency slightly decreased. The condensing vapors controlling the nucleation and growth process, sulfuric acid, and oxidation product of volatile organic compounds were estimated based on available information. The proxy values showed that sulfuric acid and organic oxidized vapors increased during the LCD period by approximately 35% and 133% on NPF days, respectively. Higher J_2 and *GR* during the LCD period were favored by the increased concentration level of condensing vapors and decreased condensation sink. Several heavy haze episodes have been reported by other studies during the LCD period; however, the increase in nanoparticle number concentration should also be considered. Some typical NPF events produced a high number concentration of nanoparticles that intensified in the following days to create severe aerosol pollution. Our study confirms a significant enhancement of the nucleation and growth process of nanoparticles during the COVID-19 LCD in Beijing and highlights the necessity of controlling nanoparticles in current and future air quality management.

1. Introduction

As a response to the outbreak of the 2019 novel coronavirus (COVID-19), the Chinese government implemented restrictions

https://doi.org/10.5194/acp-2020-1064
Preprint. Discussion started: 3 November 2020

on population movement in February 2020; the period when the restrictions were enforced was also called the lockdown period (LCD). During the LCD period, the NO_x emission was reduced by approximately 50% in China, as retrieved by the satellite (Zhang et al., 2021) and ground-based measurements (Huang et al., 2020). The number concentration of Aitken mode particles (~25-100 nm) should also decreased as expected, which related with the traffic emission (Deventer et al., 2018). The significant decrease in aerosol and precursor emissions during LCD is associated with reduced human and economic activities. However, several heavy haze pollution periods occurred in the Yangtze River Delta (YRD) and the Beijing–Tianjing–Hebei Province (BTH) region. Air pollution is driven by the enhancement of secondary particles, and NO_x reduction favors increased ozone and atmospheric oxidizing capacity (Huang et al., 2020). The aerosol heterogeneous reaction process was also enhanced by the anomalously high humidity in northern China (Le et al., 2020). Furthermore, particle accumulation was favored by stagnant airflow and vertical meteorological conditions during LCD (Zhong et al., 2020).

New particle formation (NPF) has been an active global research topic for the last two decades because of its potential climatic implications (Kulmala et al., 2004). Nucleated particles can reach number concentrations of 10^4–10^6 cm^{-3}. Subsequent growth contributes significantly to cloud condensation nuclei (CCN) (Kerminen et al., 2012) and can cause air pollution (Guo et al., 2014). Primary emissions of particulate matter (PM), CO, SO_2, and NO_2 decreased significantly after the strict clear air action plans were implemented in the last decade by the Beijing government (Zhang et al., 2019). Changes in SO_2 and background aerosols, the key factors influencing NPF events, are also linked to the formation (*J*) and growth rates (*GR*) of secondary particles (Kyrö et al., 2014). SO_2 is a key parameter governing NPF in most environments and plays an important role in nucleation and growth processes (Sihto et al., 2006, Riipinen et al., 2012). Nanoparticles (diameter ≤ 100 nm) make minor particle mass contributions but pose a serious risk to human health because of high number concentrations and deep respiratory and cardiovascular system penetration (Kawanaka et al., 2009). However, the size-resolved, chemical, and toxicological properties of nanoparticles are unclear (Jin et al., 2017). Under unfavorable meteorological conditions, the growth of the nanoparticles for several consecutive days would even probably lead to particle mass enhancement as found in Beijing, China (Guo et al., 2014).

In a previous study, the influence of NPF event occurrence by emission reduction in Beijing was analyzed for China's Victory Day parade in August 2015 and for the summer Olympics in 2008; during this period, higher NPF occurrence frequency but lower *J* and *GR* was reported as a result of low precursor concentrations (Shen et al., 2016). In the present study, we focus on changes in particle number size distribution and NPF events during LCD in Beijing and the influencing factors. The link between NPF events and regional aerosol pollution is also explored. Our study will facilitate the optimization of regulatory measures to control particle and gas pollution in China, especially with regard to the variation of NPF-associated condensing vapors caused by reduced precursor emissions and elevated atmospheric oxidizing level.

https://doi.org/10.5194/acp-2020-1064
Preprint. Discussion started: 3 November 2020

2. Methods

2.1 Measurements

The particle and ion number size distribution measurements were conducted in January and February 2020 on the roof of the Chinese Academy of Meteorological Sciences building (CAMS) on the Chinese Meteorological Administration campus. The site is approximately 53 m above ground level and located in the western Beijing urban area between the second and third ring roads. A major road with heavy traffic to the west of the site indicated that the sample air could be influenced by traffic emissions. More information about the site can be found in Wang et al. (2018).

2.2 Instrumentation

The number of particles of sizes 10–850 nm was measured using a scanning mobility particle sizer (SMPS, TROPOS, Germany). The system is a combination of a differential mobility analyzer (DMA) and a condensation particle counter (CPC, Model 3772, TSI Inc., USA). The mobility distribution of naturally charged and neutral nanoparticles is measured by a neutral cluster and air ion spectrometer (NAIS) with a 10-min time resolution (Mirme et al., 2007, Mirme and Mirme, 2013). The measured mobility was in the range 3.3–0.0013 $cm^2 V^{-1} s^{-1}$, corresponding to mobility diameters of 0.8–42 nm. Positive and negative ions were simultaneously classified by two cylindrical differential mobility analyzers (DMAs) and detected with 21 electrometers on the outer cylinder. A high sample flow rate of 60 lpm was used to minimize diffusion losses. In ion mode, the detected signal is inverted to a mobility distribution consisting of 28 bins, taking into account the measured background and experimentally determined diffusion losses. In neutral particle mode, the sample aerosol is charged using corona chargers, and the charged fraction is calculated (Fuchs, 1963). However, the lowest detection limit for the NAIS in the neutral particle mode (approximately 2 nm) was affected by the corona-generated ions (Asmi et al., 2009, Manninen et al., 2011). The lowest detection limit of the NAIS in ion mode was determined by the charging probability, nanoparticle concentration, and charger ion mobility (Kulmala et al., 2013).

The mass concentrations of $PM_{2.5}$, precursor gases of O_3, SO_2, NO_2, and CO at the GuanYuan air quality monitoring site were derived from the data center of the Ministry of Ecology and Environment of the People's Republic of China (http://datacenter.mep.gov.cn), which is 3 km from the CAMS site. The global radiation at the observatory (54511) in the southern Beijing urban area was used to estimate the sulfuric acid and OH radials as proxies in this work. The solar radiation datasets were provided by the National Meteorological Information Center of the China Meteorological Administration. The meteorological factors used in this study—wind speed (WS), wind direction (WD), and relative humidity (RH)—were derived from the Haidian National Basic Meteorological Station (54399). The data can represent meteorological conditions at the CAMS site, which is located ~5 km northwest of the urban area site.

https://doi.org/10.5194/acp-2020-1064
Preprint. Discussion started: 3 November 2020

2.3 NPF parameter calculation

The total particle and ion formation rate at 2 nm ($J_{2,tot}$ and $J_{2,ion}$) can be calculated from the particle and ion number concentrations in the size range 2–3 nm (Manninen et al., 2010, Hirsikko et al., 2011). $J_{2,tot}$ and $J_{2,ion}$ included time changes in the concentration of 2–3-nm particles or ions (first term on the right side of Eq. 1 and 2), coagulation loss of 2–3-nm particles or ions with the pre-existing particles derived by SMPS (second term), and growth of 2–3-nm particles or ions into larger sizes by the growth rate, *GR* (third term). In Eq. (2), the fourth and fifth terms represent loss due to ion–ion recombination and formation from ion-neutral attachment. The equations are given by the following formulas:

$$J_{2,tot} = \frac{dN_{2-3,tot}}{dt} + CoagS_2 \times N_{2-3,tot} + \frac{GR_3}{1nm} \times N_{2-3,tot} \quad (1)$$

$$J^{\pm}_{2,ion} = \frac{dN^{\pm}_{2-3,ion}}{dt} + CoagS_2 \times N^{\pm}_{2-3,ion} + \frac{GR_3}{1nm} N^{\pm}_{2-3,ion} + \alpha \times N^{\pm}_{2-3,ion} N^{\mp}_{<3,ion} - \beta \times N_{2-3,par} N^{\pm}_{<2,ion} \quad (2)$$

$N_{2\text{-}3,tot}$ and $N^{\pm}_{2\text{-}3,ion}$ are the number concentration of particles and ions of positive and negative charges, respectively. $CoagS_2$ is the 2-nm coagulation coefficient. α and β (the ion–ion recombination and ion-neutral attachment coefficients, respectively) are assumed to be 1.6×10^{-6} and 10^{-8} cm^3s^{-1}, respectively, (Hoppel, 1985).

Growth rate (*GR*) is defined as the rate of change of diameter with time, $GR = (D_{p,2} - D_{p,1})/dt$, given in nm h^{-1}, where $D_{p,1}$ and $D_{p,2}$ are the geometric mean diameters (GMD) when the nucleated particles start and stop growing, respectively. GMDs are derived by the log-normal modal fitting of the particle/ion number size distributions (Hussein et al., 2009).

Sulfuric acid (H_2SO_4) is a key component in the nucleation process (Kulmala et al., 2013). The concentration of H_2SO_4 was not measured directly in this study but can be estimated by the global radiation (Glob_R) and SO_2, according to the chemical mass balance model recommended by Weber et al. (1997):

$$[H_2SO_4] = \frac{k \times Glob\_R \times SO_2}{CS} \quad (3)$$

where *k* is a constant scaling coefficient that depends on the location environment and is assumed to be 1 for simplicity in the estimation. *CS* is the condensation sink, which describes how fast the vapor molecules condense on the existing particles (Dal Maso et al., 2002).

Highly oxidized biogenic organic vapors with extremely low volatility (ELVOCs) play an important role in the growth process of nucleated particles (Kulmala et al., 2014). As ELVOCs and their precursors were not available in this work, we used a surrogate method to formulate the concentration of the oxidized VOC products as follows (Kontkanen et al., 2016):

$$[VOC_{ox}] = \frac{k_{VOC,OH}[OH][VOC] + k_{VOC,O_3}[O_3][VOC]}{CS} \quad (4)$$

where $[VOC]$, $[O_3]$, and $[OH]$ are the precursor concentrations, $k_{VOC,OH}$ and k_{VOC,O_3} are the chemical rate coefficients in the daytime VOC reactions with the dominant atmospheric oxidants OH and O_3, respectively (Atkinson et al., 2006). This method

https://doi.org/10.5194/acp-2020-1064
Preprint. Discussion started: 3 November 2020

was used and validated in urban Beijing to study the contribution of VOC oxidation products to the growth of nucleated particles (Wang et al., 2015). VOC was not measured in this study; thus, we only considered the oxidization capacity variation during measurement, which was denoted as follows:

$$[VOC_{ox,capacity}] = \frac{k_{VOC,OH}[OH] + k_{VOC,O_3}[O_3]}{CS} \quad (5)$$

The concentration of OH was calculated by scaling the measured ultraviolet radiation B (UVB) radiation using the following recommended empirical equation (Petäjä et al., 2009):

$$[OH]_{proxy} = (\frac{8.4 \times 10^{-7}}{8.6 \times 10^{-10}} UVB^{0.32})^{1.92} \quad (6)$$

As with sulfuric acid estimation, global radiation (Glob_R) was applied because of the lack of UVB measurement. The concentrations of condensing vapors are estimated roughly in this work due to the lack of direct measurements of some key parameters, and thus can not represent the real level in the atmosphere, but reflect the variation trends of each parameter on NPF days during different periods.

2.4 Typical NPF event identification

NPF events are identified and different nucleation types are characterized based on the daily evolution of particle number size distribution (Dal Maso et al., 2005). Regional NPF events can occur over a geographically large area and extend over several hundreds of kilometers (Shen et al., 2018). Such events indicate regional cases in which freshly nucleated particles can reach the size of CCN (Shen et al., 2011).

3. Results and discussion

3.1 Overview of the NSD of particles and charged ions

Fig. 1 shows the time evolution of the number size distribution (NSD) of particles in the 10–850-nm range, neutral particles (2–42 nm), and charged ions (0.8–42 nm) in January and February 2020. The dataset was classified into the COVID-19 LCD (January 24–February 16, 2020), pre-LCD period (January 3–23, 2020), and post-LCD (February 17–29, 2020) to reveal the influence of emission reductions. The NPF event occurred on 10 out of 23 days (43%) during pre-LCD, 8 out of 24 days (33%) in LCD, and 5 out of 13 days (38%) in post-LCD, respectively. NPF occurrence frequency was slightly lower during LCD. Despite large primary emissions reduction, several cases of heavy aerosol pollution events occurred in the BTH region during LCD. Particle matter below 2.5 μm ($PM_{2.5}$) mass concentration at air monitoring sites in Beijing of the Ministry of Ecology and Environment of China exceeded 75 μg/m^3 (the second grade of the Ambient Air Quality Standard of China) on 12 of the 28 days. The elevated PM mass concentration was attributed to the secondary aerosol formation process; this process was aided by the enhanced oxidizing capacity caused by increased ozone levels (Huang et al., 2020). The meteorological analysis

https://doi.org/10.5194/acp-2020-1064
Preprint. Discussion started: 3 November 2020

also revealed that an inversion layer occurred in the BTH region and trapped moisture and pollutants near the ground, thus offsetting substantial emissions reductions during COVID-19 LCD (Zhong et al., 2020).

The particle number concentrations of the Aitken mode (25–100 nm, $N_{25–100nm}$) and the accumulation mode (100–850 nm, $N_{100–850nm}$) derived by SMPS and the nucleation mode (≤ 25 nm) of neutral particles and charged ions by NAIS were discussed in detail. The Aitken mode showed a significant reduction since the Chinese New Year (January 24) and normal fluctuations below 3000 cm^{-3} during LCD and post-LCD. Mean $N_{25–100}$ concentrations were 4040 ± 1590, 2400 ± 1170, and 2170 ± 994 cm^{-3} in pre-LCD, LCD, and post-LCD, respectively. Aitken mode particles were closely related to the anthropogenic emissions and reduced by approximately 40%. During post-LCD, the Aitken mode concentration remained low because people were encouraged to work at home and services were almost shut down. Accumulation mode particles usually undergo coagulation, condensation, heterogeneous reactions, and long-range transport processes that can reflect regional polluted conditions. $N_{100–850nm}$ concentrations were 1820 ± 1190, 2200 ± 1320, and 1850 ± 840 cm^{-3} during pre-LCD, LCD, and post-LCD, respectively; the 20% increase during LCD (compared with pre-LCD) occurred despite large emissions reductions and was related to specific pollution episodes that occurred from January 24–26 and February 12–14. The particle number concentration derived from SMPS is probably lower than that from NAIS in the overlap size range of 20–40 nm, because the overestimation of natural particle concentration as a multiple charge effect above 20 nm is beyond the instrumental detection limit (Gagné et al., 2011). In this study, the number concentration of 20–40 nm was integrated by the SMPS and NAIS particle mode ($N_{20–40nm,\ smps}$ and $N_{20–40nm,\ nais}$) with an enhancement factor ($N_{20–40nm,\ nais}/N_{20–40nm,\ smps}$) of 1.65 ± 0.06, and the number concentration of particles larger than 20 nm derived by SMPS was more accurate.

The nucleation mode ($N_{par,\ \leq\ 25\ nm}$) derived from NAIS was separated into ≤ 10 nm and 10–25 nm for neutral particles ($N_{par,nais,2–10nm}$, $N_{par,nais,10–25nm}$) and positively charged ions ($N_{ion,nais,1–10nm}$, $N_{ion,nais,10–25nm}$), respectively. $N_{par,nais,2–10nm}$ was the primary contributor to the nucleation mode, which was determined by NPF events, during which average peak $N_{par,nais,\leq\ 25\ nm}$ concentrations were $2.3 \pm 2.3\times10^4$, $1.5 \pm 2.6\times10^4$, and $1.9 \pm 3.3\times10^4$ cm^{-3}, during pre-LCD, LCD, and post-LCD, respectively (Fig. 2). The number concentration of 10–25-nm particles could also be derived from SMPS ($N_{par,smps,10-25nm}$), which was also given in Fig. 2 and approximately 30% lower than the value of $N_{par,nais,10-25nm}$. $N_{par,\ \leq\ 25\ nm}$ showed large variation because of significant differences between NPF and non-NPF days. However, several cases during LCD showed a significantly high peak $N_{par,2–10nm}$ value, indicating the probability of the stronger nucleation process during LCD. The positive and negative ion number concentrations of 0.8–42 nm were 457 ± 245 and 496 ± 265 cm^{-3}, respectively. The mean values of $N_{ion,nais,1–10nm}$ and $N_{ion,nais,10–25nm}$ ranged from 100–200 cm^{-3}, indicating a minor contribution to the total particle count.

3.2 NPF event variation

Table 1 provides the key parameters describing NPF events, including NPF frequency, *CS*, J_2, and *GR* for total particles and

https://doi.org/10.5194/acp-2020-1064
Preprint. Discussion started: 3 November 2020

charged ions; it shows a slightly lower frequency of NPF events during LCD. Higher J_2 and *GR* values for particles and ions were also found during LCD and post-LCD than during pre-LCD. However, the emissions control period during the China Victory Parade in Beijing in 2015 (August 20–September 3) featured higher frequency, decreasing J_3 and *GR* trends compared with the corresponding month in 2010–2013 (Shen et al., 2016). That indicated the factors influencing the NPF event, including precursors, pre-existing particles and meteorological conditions, were complex and should be evaluated further. In this study, the daily mean value of NO_2 decreased by ~35% and SO_2 decreased by ~13%, whereas O_3 increased by 80% during LCD as compared to pre-LCD (Fig. 3). The previous study indicated that NO_x suppresses NPF events by influencing the formation of highly oxygenated organic molecules (HOMs), which participated in nucleation and initial particle growth (Lehtipalo et al., 2018, Yan et al., 2020), suggesting that the reduction of NO_2 during LCD provided favorable conditions for particle growth. O_3, an important atmospheric oxidant, increased during LCD because of the large reduction in NO_x emissions (Huang et al., 2020). In general, the variations of precursors and *CS* could finally influence NPF by photochemical reactions with VOCs and sulfuric acid production as discussed in the following section.

The H_2SO_4 and low-volatility organic vapor proxy were derived according to equations (3–6); Fig. 4 presents the estimated values. As discussed separately for LCD and pre-LCD during the NPF event occurrence (9:00–16:00 LT), *CS* decreased by ~25% and Glob_R increased by ~40%, whereas SO_2 decreased by ~28%. The variations of these variables finally lead to a H_2SO_4 increase of ~35%. The formation of sulfuric acid was aided by the enhanced atmospheric oxidizing capacity because of elevated O_3 concentration during LCD, which had also been validated in the previous study in Nanjing, YRD, China (Huang et al., 2020). It also reported that VOC emissions in the BTH region were reduced by ~45% (Huang et al., 2020), but oxidized capacity was enhanced by ~50% based on our estimation during LCD period. Especially on NPF days, the VOC oxidization capacity enhancement factor was ~1.3. Thus, the oxidization product with low volatility probably increased and offset the reduction of VOC emissions, and favored particle growth. These results are consistent with those of a previous study showing that elevated O_3 promoted SO_2 oxidation into sulfate and VOCs into low-volatility vapors, which condensed onto the particle surface and contributed to the nucleation and growth process (Ehn et al., 2014).

The correlation between the H_2SO_4 proxy and $J_{2,tot}$ (*GR*) was indicated by different $VOC_{ox,capacity}$ levels as shown in Fig. 5. *GR* showed higher values corresponding to high concentrations of condensing vapors. The correlation coefficient (*R*) was 0.56 for $J_{2,tot}$ and the H_2SO_4 proxy, and 0.62 for *GR* and the H_2SO_4 proxy, respectively. *R* was 0.74 and 0.60, respectively, for the correlation between $J_{2,tot}$ and $VOC_{ox,capacity}$ and *GR* and $VOC_{ox,capacity}$, respectively. The non-linear dependence of $J_{2,tot}$, and *GR* on the condensing vapors indicates a complex mechanism in the multi-component nucleation and growth system. When the particles overcame the criteria size of 10 nm, sulfuric acid—which plays an important role in smaller growth processes from 2–10 nm—could not explain condensational growth (Stolzenburg et al., 2020). For particles larger than 10 nm, low volatile

https://doi.org/10.5194/acp-2020-1064
Preprint. Discussion started: 3 November 2020

organic vapors should contribute to growth (Kontkanen et al., 2018, Yan et al., 2020). The general increase in J_2 and *GR* during LCD compared with pre-LCD was probably related to the increase in the sulfuric acid concentration and VOC oxidization capacity.

3.3 Effect of charged ions

Table 1 provides the parameters describing the nucleation and growth process for neutral particles and positive and negative ions and shows that the *GR* of ions was larger than that of neutral particles. The growth of the nano-sized particles was not linear (especially at the initial size); therefore, the *GR* calculation was split into different size ranges (Fig. 6). The *GR* of charged ions was higher than that of neutral particles for all size ranges, which is consistent with previous studies (Hirsikko et al., 2005, Suni et al., 2008), and the difference was much larger at initial sizes below 5 nm. In addition to condensational growth, the difference in the loss rates of smaller particles (neutral, positive, negative) due to the coagulation process and ion–ion recombination also affects particle size and calculated *GRs* (Yu and Turco, 2008, 2011). Growth enhancement from charge–dipole interactions between condensable gases and charged ions lead to higher growth rates than with neutral particles (Yu and Turco, 2000, Nadykto and Yu, 2003). The enhancement factor due to the charge effect was 1.35 ± 0.35 during the entire particle growth process and higher (~2.0) for the initial size of 2–5 nm. These results were comparable with the experimental laboratory demonstration of an enhancement factor of 1.8–3.2 nm due to the charge effect (Stolzenburg et al., 2020). The effect of the charger decreases as particle size increases, and more species condense as particles grow. However, the number concentration of charged ions plays a minor role in the total particle count, and their contribution to the total growth process and nucleation can be ignored in urban Beijing, where the nucleation mechanism is dominated by neutral pathway with abundant condensing vapors.

3.4 Air pollution episode followed by NPF event

Two severe pollution episodes occurred during LCD from January 24–29 and February 7–14, with daily average $PM_{2.5}$ mass concentrations in the range 75–210 μg/m^3. Both episodes occurred after NPF days on January 23 (No. 10) and February 4 (No. 15), respectively. Other pollution episodes in January 16–18, February 19–21, and February 28–29 were preceded by NPF events No. 8, 21, and 23, respectively. The most long-lasting pollution episode on February 7–14 is discussed further to reveal the relationship between NPF events and aerosol pollution formation (Fig. 7). The NPF events on February 4–5 produced high concentrations of nucleation mode particles, which grew to 150–200 nm in a few days. Two principal pollution episode formation stages were identified according to variations in the $PM_{2.5}$ mass concentration dividing by CO ($PM_{2.5}$/CO). The normalized $PM_{2.5}$ by CO represents the secondary aerosol formation effect, which segregates the possible influence of physical effects, such as air mass change and boundary layer development (Wiedensohler et al., 2009). In the first stage (February 5–

https://doi.org/10.5194/acp-2020-1064
Preprint. Discussion started: 3 November 2020

11), the secondary aerosol formation was the key process contributing to increasing $PM_{2.5}$ mass. As in the second stage (February 11–13), $PM_{2.5}$ reached a peak value of 250 μg/m^3, and $PM_{2.5}$/CO slightly decreased with small fluctuations. Because primary emission should not change during this period, and unfavorable meteorological conditions could be responsible for the event. During this period, northeasterly and southwesterly winds were dominant, whereas the WS was normally lower than 2 m/s. RH remained high (from 80% to >90%) from February 5–14 with a few hours of RH <60% during the daytime. Particle hygroscopic growth under high ambient RH conditions and heterogeneous reactions on particle surfaces could also contribute to the elevated particle mass concentration (Wang et al., 2018). Consequently, nucleated particles accumulated because of enhanced oxidizing capacity and favorable meteorological conditions and caused severe aerosol pollution.

4. Conclusion

In this study, we presented changes in the NSD of particles and charged ions measured in January and February 2020 to reveal the influence of emission reduction on NPF events. Particles smaller than 100 nm were effectively reduced by ~40% because of suspended human activities during the Chinese New Year and the COVID-19 LCD. The accumulation mode particles were slightly higher during LCD, as several hazy days were associated with secondary aerosol formation. The frequency of NPF days was slightly lower during LCD as compared with pre_LCD period; however, J_2 and *GR* were significantly higher. Enhanced formation and growth rates were related to the elevated oxidation capacity of the atmosphere, which could be seen from the increase of sulfuric acid concentration proxy and VOC oxidization capacity. During LCD, NO_x and SO_2 concentrations decreased as anthropogenic emissions were reduced. Higher O_3 and a lower condensation sink raised sulfuric acid concentration levels by ~35% and VOC oxidization capacity by a factor of 1.3 on NPF days, which were responsible for the higher nucleation rate and larger nanoparticle quantity. The elevated sulfuric acid concentration and VOC oxidization capacity could explain the higher $J_{2,tot}$ and *GR* to some extent. The nucleated particles entered accumulation mode by the secondary aerosol formation and underwent hygroscopic growth under high RH and calm wind conditions, which facilitated the occurrence of severe pollution episodes during LCD. This work highlights the potential influence of strict emission control strategies on NPF events and provides insights into the positive and negative effects of precursors and atmospheric oxidizing capacity on the nucleation and growth process of the nanoparticles.

Data availability. All the data related to this paper may be requested from the corresponding author: shenxj@cma.gov.cn.

Author contributions. XS and JS designed the research and led the overall scientific questions. XS, JZ, YZ, CX, XH and SZ carried out the field experiment, data processing and analysis. XS wrote the first draft of the manuscript and FY, XZ revised the manuscript. All authors read and approved the final version.

Competing interests. The authors declare that they have no conflict of interest.

Acknowledgement. This research was supported by the National Natural Science Foundation of China (41875147, 42075082, 41675129) and the Chinese Academy of Meteorological Sciences (2020KJ001). It was also supported by the Innovation Team for Haze-fog Observation and Forecasts of MOST and CMA.

References

Asmi, A., Sipilä, M., Manninen, H. E., Vanhanen, J., Lehtipalo, K., Gagné, S., Neitola, K., Mirme, A., Mirme, S., E, T., Uin, J., Komsaare, K., Attoui, M. and Kulmala, M.: Results of the first air ion spectrometer calibration and intercomparison workshop, Atmos. Chem. Phys., 9: 141-154, 2009.

Atkinson, R., Baulch, D. L., Cox, R. A., Crowley, J. N., Hampson, R. F., Hynes, R. G., Jenkin, M. E., Rossi, M. J., Troe, J. and Subcommittee, I.: Evaluated kinetic and photochemical data for atmospheric chemistry: Volume II - gas phase reactions of organic species, Atmos. Chem. Phys., 6(11): 3625-4055, DOI: 10.5194/acp-6-3625-2006, 2006.

Dal Maso, M., Kulmala, M., Lehtinen, K. E. J., Mäkelä, J. M., Aalto, P. and O'Dowd, C. D.: Condensation and coagulation sinks and formation of nucleation mode particles in coastal and boreal forest boundary layers, J. Geophys. Res., 107(D19): 10.1029/2001JD001053, 2002.

Dal Maso, M., Kulmala, M., Riipinen, I., Wagner, R., Hussein, T., Aalto, P. P. and Lehtinen, K. E. J.: Formation and growth of fresh atmospheric aerosols: eight years of aerosol size distribution data from SMEAR II, Boreal Environ. Res., 10: 323–336, 2005.

Deventer, M. J., von der Heyden, L., Lamprecht, C., Graus, M., Karl, T. and Held, A.: Aerosol particles during the Innsbruck Air Quality Study (INNAQS): Fluxes of nucleation to accumulation mode particles in relation to selective urban tracers, Atmos. Environ., 190: 376-388, DOI: 10.1016/j.atmosenv.2018.04.043, 2018.

Ehn, M., Thornton, J. A., Kleist, E., Sipila, M., Junninen, H., Pullinen, I., Springer, M., Rubach, F., Tillmann, R., Lee, B., Lopez-Hilfiker, F., Andres, S., Acir, I. H., Rissanen, M., Jokinen, T., Schobesberger, S., Kangasluoma, J., Kontkanen, J., Nieminen, T., Kurten, T., Nielsen, L. B., Jorgensen, S., Kjaergaard, H. G., Canagaratna, M., Maso, M. D., Berndt, T., Petaja, T., Wahner, A., Kerminen, V. M., Kulmala, M., Worsnop, D. R., Wildt, J. and Mentel, T. F.: A large source of low-volatility secondary organic aerosol, Nature, 506(7489): 476-479, DOI: 10.1038/nature13032, 2014.

Fuchs, N. A.: On the stationary charge distribution on aerosol particles in bipolar ionic atmosphere, Geofis. Pura Appl., 56: 185-193, 1963.

Gagné, S., Lehtipalo, K., Manninen, H. E., Nieminen, T., Schobesberger, S., Franchin, A., Yli-Juuti, T., Boulon, J., Sonntag, A., Mirme, S., Mirme, A., Hõrrak, U., Petäjä, T., Asmi, E. and Kulmala, M.: Intercomparison of air ion spectrometers: an evaluation of results in varying conditions, Atmos. Meas. Tech., 4(5): 805-822, DOI: 10.5194/amt-4-805-2011, 2011.

https://doi.org/10.5194/acp-2020-1064
Preprint. Discussion started: 3 November 2020

Guo, S., Hu, M., Zamora, M. L., Peng, J., Shang, D., Zheng, J., Du, Z., Wu, Z., Shao, M., Zeng, L., Molina, M. J. and Zhang, R.: Elucidating severe urban haze formation in China, Proc Natl Acad Sci, 111(49): 17373-17378, DOI: 10.1073/pnas.1419604111, 2014.

Hirsikko, A., Laakso, L., Aalto, P. P., Kerminen, V.-M., Hõrrak, U. and Kulmala, M.: Annual and size dependent variation of growth rates and ion concentrations in boreal forest, Boreal Envrion. Res., 10: 357–369, 2005.

Hirsikko, A., Nieminen, T., Gagné, S., Lehtipalo, K., Manninen, H. E., Ehn, M., Hõrrak, U., Kerminen, V. M., Laakso, L., McMurry, P. H., Mirme, A., Mirme, S., Petäjä, T., Tammet, H., Vakkari, V., Vana, M. and Kulmala, M.: Atmospheric ions and nucleation: a review of observations, Atmos. Chem. Phys., 11(2): 767-798, DOI: 10.5194/acp-11-767-2011, 2011.

Hoppel, W. A.: Ion-Aerosol Attachement Coefficients, Ion Depletion, and the Charge Distribution on Aerosols, J. Geophys. Res., 90: 5917–5923, 1985.

Huang, X., Ding, A., Gao, J., B. Zheng, D. Zhou, X. Qi, R. Tang, J. Wang, C. Ren, W. Nie, X. Chi, Z. Xu, L. Chen, Y. Li, F. Che, N. Pang, H. Wang, D. Tong, W. Qin, W. Cheng, W. Liu, Q. Fu, B. Liu, F. Chai, S.J. Davis, Q. Zhang and K. He. Enhanced secondary pollution offset reduction of primary emissions during COVID-19 lockdown in China, National Sci Rev, nwaa137, 2020.

Hussein, T., Junninen, H., Tunved, P., Kristensson, A., Maso, M. D., Riipinen, I., Aalto, P. P., Hansson, H.-C., Swietlicki, E. and Kulmala, M.: Time span and spatial scale of regional new particle formation events over Finland and Southern Sweden, Atmos. Chem. Phys., 9: 4699–4716, 2009.

Jin, L., Luo, X., Fu, P. and Li, X.: Airborne particulate matter pollution in urban China: a chemical mixture perspective from sources to impacts, National Sci Rev, 4(4): 593-610, DOI: 10.1093/nsr/nww079, 2017.

Kawanaka, Y., Tsuchiya, Y., Yun, S. J. and Sakamoto, K.: Size distributions of polycyclic aromatic hydrocarbons in the atmosphere and estimation of the contribution of ultrafine particles to their lung deposition, Environ Sci Technol, 43: 6851–6856, 2009.

Kerminen, V. M., Paramonov, M., Anttila, T., Riipinen, I., Fountoukis, C., Korhonen, H., Asmi, E., Laakso, L., Lihavainen, H., Swietlicki, E., Svenningsson, B., Asmi, A., Pandis, S. N., Kulmala, M. and Petäjä, T.: Cloud condensation nuclei production associated with atmospheric nucleation: a synthesis based on existing literature and new results, Atmos. Chem. Phys., 12(24): 12037-12059, DOI: 10.5194/acp-12-12037-2012, 2012.

Kontkanen, J., Olenius, T., Kulmala, M. and Riipinen, I.: Exploring the potential of nano-Köhler theory to describe the growth of atmospheric molecular clusters by organic vapors using cluster kinetics simulations, Atmos. Chem. Phys., 18(18): 13733-13754, DOI: 10.5194/acp-18-13733-2018, 2018.

Kontkanen, J., Paasonen, P., Aalto, J., Bäck, J., Rantala, P., Petäjä, T. and Kulmala, M.: Simple proxies for estimating the

concentrations of monoterpenes and their oxidation products at a boreal forest site, Atmos. Chem. Phys., 16(20): 13291-13307, DOI: 10.5194/acp-16-13291-2016, 2016.

Kulmala, M., Kontkanen, J., Junninen, H., Lehtipalo, K., Manninen, H. E., Nieminen, T., Petaja, T., Sipila, M., Schobesberger, S., Rantala, P., Franchin, A., Jokinen, T., Jarvinen, E., Aijala, M., Kangasluoma, J., Hakala, J., Aalto, P. P., Paasonen, P., Mikkila, J., Vanhanen, J., Aalto, J., Hakola, H., Makkonen, U., Ruuskanen, T., Mauldin, R. L., Duplissy, J., Vehkamaki, H., Back, J., Kortelainen, A., Riipinen, I., Kurten, T., Johnston, M. V., Smith, J. N., Ehn, M., Mentel, T. F., Lehtinen, K. E. J., Laaksonen, A., Kerminen, V. M. and Worsnop, D. R.: Direct Observations of Atmospheric Aerosol Nucleation, Science, 339(6122): 943-946, DOI: 10.1126/science.1227385, 2013.

Kulmala, M., Petäjä, T., Ehn, M., Thornton, J., Sipilä, M., Worsnop, D. R. and Kerminen, V.-M.: Chemistry of Atmospheric Nucleation: On the Recent Advances on Precursor Characterization and Atmospheric Cluster Composition in Connection with Atmospheric New Particle Formation, Annu Rev Phys Chem, 65(1): 21-37, DOI: 10.1146/annurev-physchem-040412-110014, 2014.

Kulmala, M., Vehkamäki, H., Petäjä, T., Dal Maso, M., Lauri, A., Kerminen, V. M., Birmili, W. and McMurry, P. H.: Formation and growth rates of ultrafine atmospheric particles: a review of observations, J. Aerosol Sci., 35(2): 143-176, DOI: 10.1016/j.jaerosci.2003.10.003, 2004.

Kyrö, E. M., Väänänen, R., Kerminen, V. M., Virkkula, A., Petäjä, T., Asmi, A., Dal Maso, M., Nieminen, T., Juhola, S., Shcherbinin, A., Riipinen, I., Lehtipalo, K., Keronen, P., Aalto, P. P., Hari, P. and Kulmala, M.: Trends in new particle formation in eastern Lapland, Finland: effect of decreasing sulfur emissions from Kola Peninsula, Atmos. Chem. Phys., 14(9): 4383-4396, DOI: 10.5194/acp-14-4383-2014, 2014.

Le, T., Wang, Y., Liu, L., Yang, J., Yung, Y. L., Li, G. and Seinfeld, J. H.: Unexpected air pollution with marked emission reductions during the COVID-19 outbreak in China, Science, 10.1126/science.abb7431, 2020.

Lehtipalo, K., Yan, C., Dada, L., Bianchi, F., Xiao, M., Wagner, R., Stolzenburg, D., Ahonen, L. R., Amorim, A., Baccarini, A., Bauer, P. S., Baumgartner, B. and Bergen, A.: Multicomponent new particle formation from sulfuric acid, ammonia, and biogenic vapors, Science Advance, 4: eaau5363, 2018.

Manninen, H. E., Franchin, A., Schobesberger, S., Hirsikko, A., Hakala, J., Skromulis, A., Kangasluoma, J., Ehn, M., Junninen, H., Mirme, A., Mirme, S., Sipilä, M., Petäjä, T., Worsnop, D. R. and Kulmala, M.: Characterisation of corona-generated ions used in a Neutral cluster and Air Ion Spectrometer (NAIS), Atmos. Meas. Tech., 4(12): 2767-2776, DOI: 10.5194/amt-4-2767-2011, 2011.

Manninen, H. E., Nieminen, T., Asmi, E., Gagné, S., Häkkinen, S., Lehtipalo, K., Aalto, P., Vana, M., Mirme, A., Mirme, S., Hõrrak, U., Plass-Dülmer, C., Stange, G., Kiss, G., Hoffer, A., Törő, N., Moerman, M., Henzing, B., de Leeuw, G., Brinkenberg,

M., Kouvarakis, G. N., Bougiatioti, A., Mihalopoulos, N., O'Dowd, C., Ceburnis, D., Arneth, A., Svenningsson, B., Swietlicki, E., Tarozzi, L., Decesari, S., Facchini, M. C., Birmili, W., Sonntag, A., Wiedensohler, A., Boulon, J., Sellegri, K., Laj, P., Gysel, M., Bukowiecki, N., Weingartner, E., Wehrle, G., Laaksonen, A., Hamed, A., Joutsensaari, J., Petäjä, T., Kerminen, V. M. and Kulmala, M.: EUCAARI ion spectrometer measurements at 12 European sites – analysis of new particle formation events, Atmos. Chem. Phys., 10(16): 7907-7927, DOI: 10.5194/acp-10-7907-2010, 2010.

Mirme, A., Tamm, E., Mordas, G., Vana, M., Uin, J., Mirme, S., Bernotas, T., Laakso, L., Hirsikko, A. and Kulmala, M.: A wide- range multi-channel Air Ion Spectrometer, Boreal Environ. Res., 12: 247–264, 2007.

Mirme, S. and Mirme, A.: The mathematical principles and design of the NAIS – a spectrometer for the measurement of cluster ion and nanometer aerosol size distributions, Atmos. Meas. Tech., 6(4): 1061-1071, DOI: 10.5194/amt-6-1061-2013, 2013.

Nadykto, A. B. and Yu, F.: Uptake of neutral polar vapor molecules by charged clusters/particles: Enhancement due to dipole-charge interaction, J. Geophys. Res., 108(D23), DOI: 10.1029/2003jd003664, 2003.

Petäjä, T., Mauldin, I. R. L., Kosciuch, E., McGrath, J., Nieminen, T., Paasonen, P., Boy, M., Adamov, A., Kotiaho, T. and Kulmala, M.: Sulfuric acid and OH concentrations in a boreal forest site, Atmos. Chem. Phys., 9(19): 7435-7448, DOI: 10.5194/acp-9-7435-2009, 2009.

Riipinen, I., Yli-Juuti, T., Pierce, J. R., Petäjä, T., Worsnop, D. R., Kulmala, M. and Donahue, N. M.: The contribution of organics to atmospheric nanoparticle growth, Nature Geoscience, 5(7): 453-458, DOI: 10.1038/ngeo1499, 2012.

Shen, X. J., Sun, J., Kivekäs, N., Kristensson, A., Zhang, X., Zhang, Y., Zhang, L., Fan, R., Qi, X., Ma, Q. and Zhou, H.: Spatial distribution and occurrence probability of regional new particle formation events in eastern China, Atmos. Chem. Phys., 18(2): 587-599, DOI: 10.5194/acp-18-587-2018, 2018.

Shen, X. J., Sun, J. Y., Zhang, X. Y., Zhang, Y. M., Zhang, L., Fan, R. X., Zhang, Z. X., Zhang, X. L., Zhou, H. G., Zhou, L. Y., Dong, F. and Shi, Q. F.: The influence of emission control on particle number size distribution and new particle formation during China's V-Day parade in 2015, Sci Total Environ, 573: 409-419, DOI: 10.1016/j.scitotenv.2016.08.085, 2016.

Shen, X. J., Sun, J. Y., Zhang, Y. M., Wehner, B., Nowak, A., Tuch, T., Zhang, X. C., Wang, T. T., Zhou, H. G., Zhang, X. L., Dong, F., Birmili, W. and Wiedensohler, A.: First long-term study of particle number size distributions and new particle formation events of regional aerosol in the North China Plain, Atmos. Chem. Phys., 11(4): 1565-1580, DOI: 10.5194/acp-11-1565-2011, 2011.

Sihto, S.-L., Kulmala, M., Kerminen, V.-M., Maso, M. D., Petäjä, T., Riipinen, I., Korhonen, H., Arnold, F., Janson, R., Boy, M., Laaksonen, A. and Lehtinen, K. E. J.: Atmospheric sulphuric acid and aerosol formation: implications from atmospheric measurements for nucleation and early growth mechanisms, Atmos. Chem. Phys., 6: 4079–4091, 2006.

Stolzenburg, D., Simon, M., Ranjithkumar, A., Kürten, A., Lehtipalo, K., Gordon, H., Ehrhart, S., Finkenzeller, H.,

https://doi.org/10.5194/acp-2020-1064
Preprint. Discussion started: 3 November 2020

Pichelstorfer, L., Nieminen, T., He, X.-C., Brilke, S., Xiao, M., Amorim, A., Baalbaki, R., Baccarini, A., Beck, L., Bräkling, S., Caudillo Murillo, L., Chen, D., Chu, B., Dada, L., Dias, A., Dommen, J., Duplissy, J., El Haddad, I., Fischer, L., Gonzalez Carracedo, L., Heinritzi, M., Kim, C., Koenig, T. K., Kong, W., Lamkaddam, H., Lee, C. P., Leiminger, M., Li, Z., Makhmutov, V., Manninen, H. E., Marie, G., Marten, R., Müller, T., Nie, W., Partoll, E., Petäjä, T., Pfeifer, J., Philippov, M., Rissanen, M. P., Rörup, B., Schobesberger, S., Schuchmann, S., Shen, J., Sipilä, M., Steiner, G., Stozhkov, Y., Tauber, C., Tham, Y. J., Tomé, A., Vazquez-Pufleau, M., Wagner, A. C., Wang, M., Wang, Y., Weber, S. K., Wimmer, D., Wlasits, P. J., Wu, Y., Ye, Q., Zauner-Wieczorek, M., Baltensperger, U., Carslaw, K. S., Curtius, J., Donahue, N. M., Flagan, R. C., Hansel, A., Kulmala, M., Lelieveld, J., Volkamer, R., Kirkby, J. and Winkler, P. M.: Enhanced growth rate of atmospheric particles from sulfuric acid, Atmos. Chem. Phys., 20(12): 7359-7372, DOI: 10.5194/acp-20-7359-2020, 2020.

Suni, T., Kulmala, M., Hirsikko, A., Bergman, T., Laakso, L., Aalto, P. P., Leuning, R., Cleugh, H., Zegelin, S., Hughes, D., Gorsel, E. v., Kitchen, M., Vana, M., H˜orrak, U., Mirme, S., Mirme, A., Sevanto, S., Twining, J. and Tadros, C.: Formation and characteristics of ions and charged aerosol particles in a native Australian Eucalypt forest, Atmos. Chem. Phys, 8: 129–139, 2008.

Wang, X., Shen, X. J., Sun, J. Y., Zhang, X. Y., Wang, Y. Q., Zhang, Y. M., Wang, P., Xia, C., Qi, X. F. and Zhong, J. T.: Size-resolved hygroscopic behavior of atmospheric aerosols during heavy aerosol pollution episodes in Beijing in December 2016, Atmos. Environ., 194: 188-197, DOI: 10.1016/j.atmosenv.2018.09.041, 2018.

Wang, Z. B., Hu, M., Pei, X. Y., Zhang, R. Y., Paasonen, P., Zheng, J., Yue, D. L., Wu, Z. J., Boy, M. and Wiedensohler, A.: Connection of organics to atmospheric new particle formation and growth at an urban site of Beijing, Atmos. Environ., 103: 7-17, DOI: 10.1016/j.atmosenv.2014.11.069, 2015.

Weber, R. J., Marti, J. J., McMurry, P. H., Eisele, F. L., Tanner, D. J. and Jefferson, A.: Measurements of new particle formation and ultrafine particle growth rates at a clean continental site, J. Geophys. Res, 102(D4): 4375, DOI: 10.1029/96jd03656, 1997.

Wiedensohler, A., Cheng, Y. F., Nowak, A., Wehner, B., Achtert, P., Berghof, M., Birmili, W., Wu, Z. J., Hu, M., Zhu, T., Takegawa, N., Kita, K., Kondo, Y., Lou, S. R., Hofzumahaus, A., Holland, F., Wahner, A., Gunthe, S. S., Rose, D., Su, H. and Pöschl, U.: Rapid aerosol particle growth and increase of cloud condensation nucleus activity by secondary aerosol formation and condensation: A case study for regional air pollution in northeastern China, J. Geophys. Res., 114, DOI: 10.1029/2008jd010884, 2009.

Yan, C., Nie, W., Vogel, A. L., Dada, L., Lehtipalo, K., Stolzenburg, D., Wagner, R., Rissanen, M. P., Xiao, M., Ahonen, L., Fischer, L., Rose, C., Bianchi, F., Gordon, H., Simon, M. and Heinritzi, M.: Size-dependent influence of NOx on the growth rates of organic aerosol particles, Science Advance, 6: eaay4945, 2020.

Yu, F. and Turco, R.: Case studies of particle formation events observed in boreal forests: implications for nucleation

https://doi.org/10.5194/acp-2020-1064
Preprint. Discussion started: 3 November 2020

mechanisms, Atmos. Chem. Phys., 8: 6085–6102, 2008.

Yu, F. and Turco, R. P.: The size-dependent charge fraction of sub-3-nm particles as a key diagnostic of competitive nucleation mechanisms under atmospheric conditions, Atmos. Chem. Phys., 11(18): 9451-9463, DOI: 10.5194/acp-11-9451-2011, 2011.

Yu, F. Q. and Turco, R. P.: Ultrafine aerosol formation via ion-mediated nucleation, Geophys. Res. Lett., 27(6): 883-886, DOI: 10.1029/1999gl011151, 2000.

Zhang, Q., Pan, Y., He, Y., Walters, W. W., Ni, Q., Liu, X., Xu, G., Shao, J. and Jiang, C.: Substantial nitrogen oxides emission reduction from China due to COVID-19 and its impact on surface ozone and aerosol pollution, Sci Total Environ, 753, DOI: 10.1016/j.scitotenv.2020.142238, 2021.

Zhang, X. Y., Xu, X. D., Ding, Y. H., Liu, Y. J., Zhang, H. D., Wang, Y. Q. and Zhong, J. T.: The impact of meteorological changes from 2013 to 2017 on PM2.5 mass reduction in key regions in China, Science China Earth Sciences, 62(12): 1885–1902, 2019.

Zhong, J., Zhang, X., Wang, Y. and Shen, X.: Classifying, evaluating, and predicting vertical conditions associated with PM2.5 pollution using time-series clustering, In Preparation, 2020.

Table 1. Parameters characterizing NPF events during pre-LCD, LCD, and post-LCD, including NPF frequency, formation rate ($J_{2,par}$, J_{2,pos_ion}, J_{2,neg_ion}) and growth rate ($GR_{2,par}$, GR_{pos_ion}, GR_{neg_ion}) of the total particles and charge ions, as well as condensation sink (*CS*).

	Pre-LCD	LCD	Post-LCD
NPF frequency	43%	33%	38%
$J_{2,par}$ ($cm^{-3}s^{-1}$)	5.6 ± 2.3	7.9 ± 4.5	5.9 ± 3.5
J_{2,pos_ion} ($cm^{-3}s^{-1}$)	0.010 ± 0.003	0.032 ± 0.003	0.021 ± 0.014
J_{2,neg_ion} ($cm^{-3}s^{-1}$)	0.009 ± 0.004	0.024 ± 0.005	0.015 ± 0.011
GR_{par} (nm h^{-1})	0.8 ± 0.5	1.5 ± 0.7	2.0 ± 0.5
GR_{pos_ion} (nm h^{-1})	1.8 ± 0.3	3.1 ± 0.2	3.6 ± 0.4
GR_{neg_ion} (nm h^{-1})	2.0 ± 0.7	3.1 ± 0.4	3.2 ± 0.4
CS (s^{-1})	0.010 ± 0.003	0.008 ± 0.006	0.008 ± 0.003

https://doi.org/10.5194/acp-2020-1064
Preprint. Discussion started: 3 November 2020

Atmospheric Chemistry and Physics Discussions

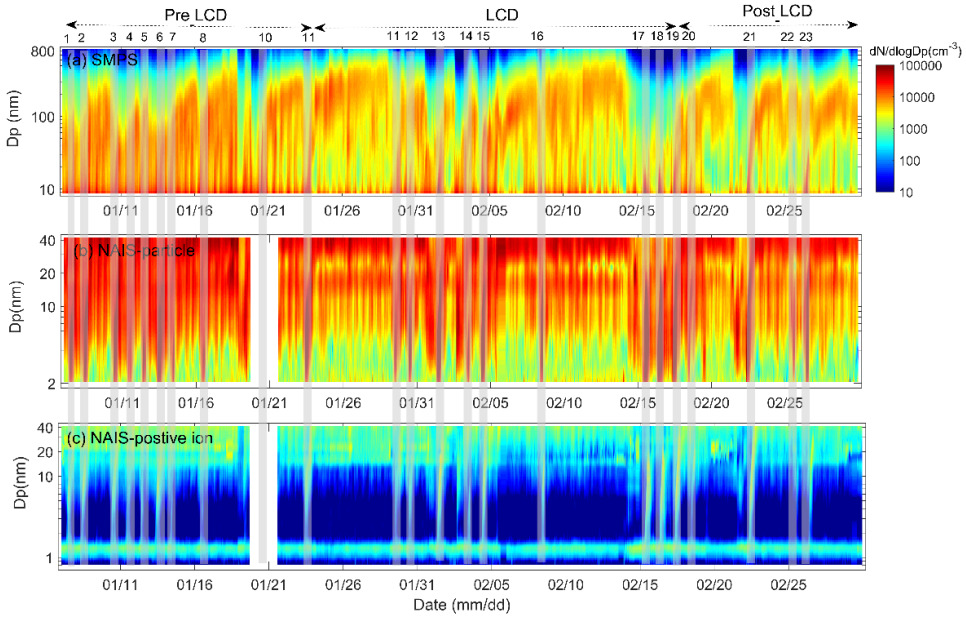

435 Fig. 1. Time evolution of number size distribution of 10–850-nm particles by SMPS (a), neutral 2–42-nm particles by NAIS in positive particle mode (b), and positive 0.8–42-nm ions by NAIS (c). NPF events were marked by numbers from 1–23.

Fig. 2. Time series of hourly mean of the number concentrations for different size ranges, including 25–100 nm and 100–850 nm, from SMPS data (a); 2–10 nm particles from NAIS and 10–25 nm particles from both NAIS and SMPS

https://doi.org/10.5194/acp-2020-1064
Preprint. Discussion started: 3 November 2020

(b); 1–10 nm and 10–25 nm positive ions from NAIS (c).

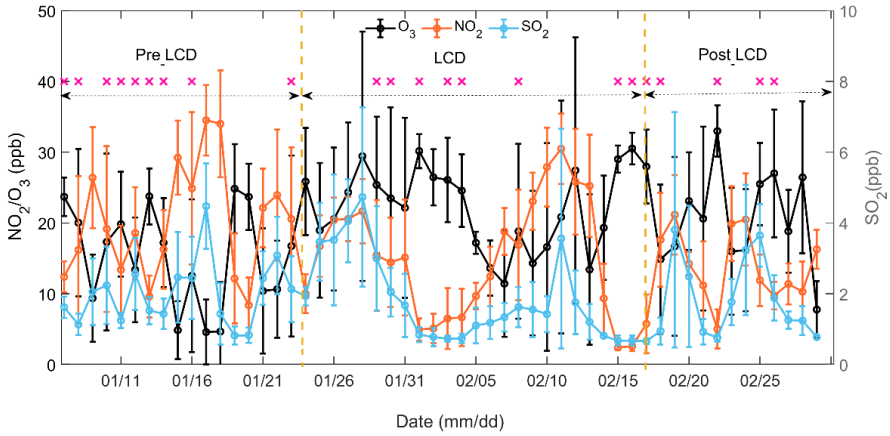

Fig. 3. Concentration level of precursors, including NO_2 (a), SO_2 (b), and O_3 (c) during the measurement period. The circle and bar indicate the mean and standard deviation, respectively; NPF days are marked with a pink cross.

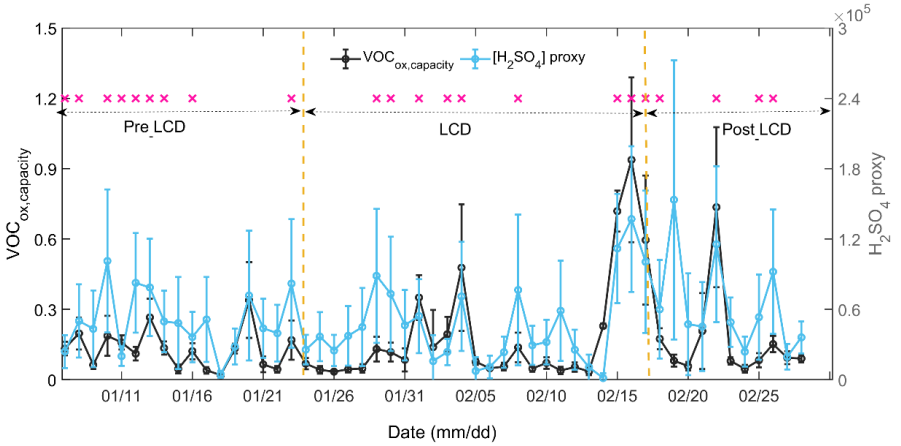

Fig. 4. Estimated oxidized capacity of the VOC (VOCox, capacity) and sulfuric acid proxy (H_2SO_4) during pre-LCD, LCD and post-LCD, respectively. The circle and bar indicate the mean and standard deviation, respectively; NPF days are marked with a pink cross.

https://doi.org/10.5194/acp-2020-1064
Preprint. Discussion started: 3 November 2020

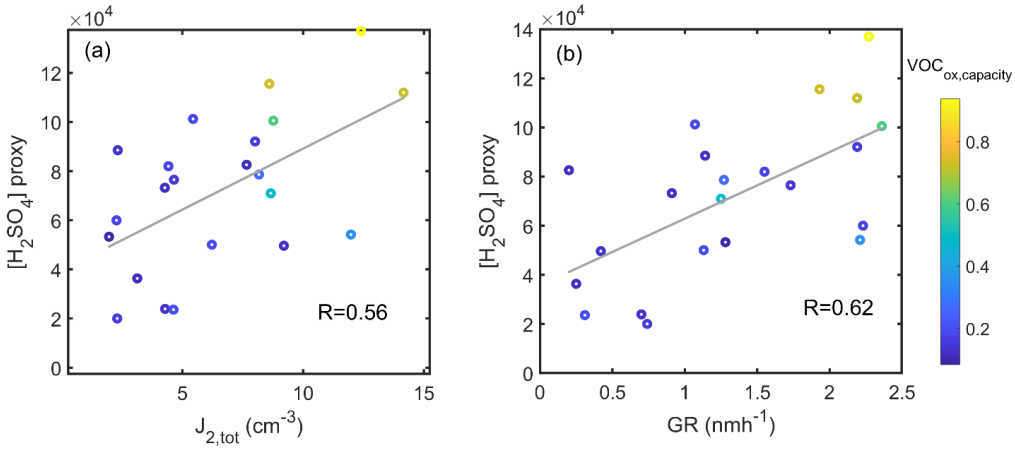

Fig. 5. Scatter plot of *J* (a) and *GR* (b) versus the proxy of sulfuric acid and VOC oxidization capacity ($VOC_{ox,capicity}$) for all NPF events. The color of the circles indicates the level of $VOC_{ox,capacity}$. The linear fit lines (gray) and correlation coefficient (*R*) are given.

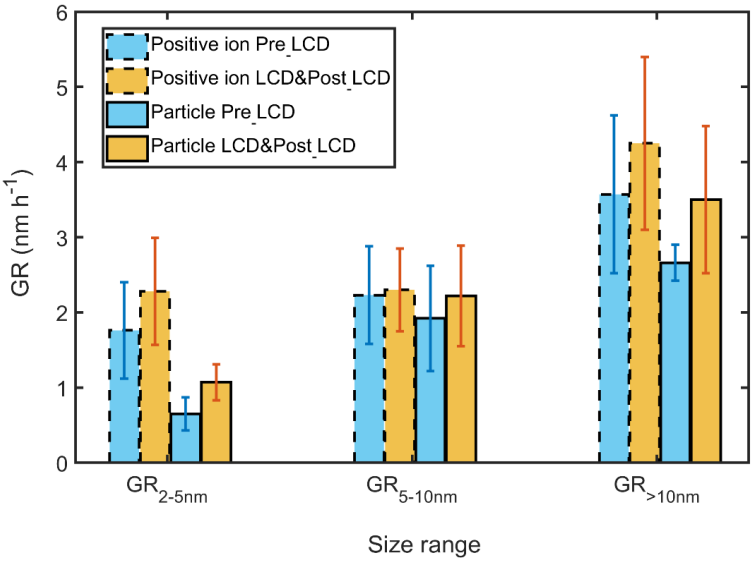

Fig. 6. Growth rates of particles and ions in different size ranges, including 2–5 nm ($GR_{2–5nm}$), 5–10 nm ($GR_{5–10nm}$), and >10 nm ($GR_{>10nm}$), during Pre_LCD and LCD&Post_LCD, respectively.

https://doi.org/10.5194/acp-2020-1064
Preprint. Discussion started: 3 November 2020

Atmospheric Chemistry and Physics Discussions

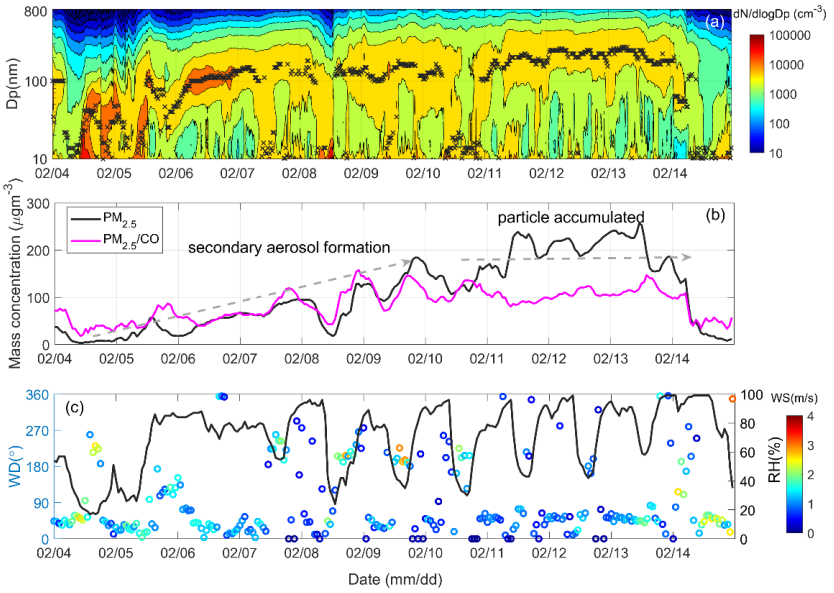

Fig. 7. Time evolution of PNSD and the dominant geometric mean diameters (black cross) derived by the log-modal fitting (a) and hourly mean $PM_{2.5}$ (black line), normalized $PM_{2.5}$ by CO (pink line) in (b) and the meteorological factors: wind direction (WD), wind speed (WS), and relative humidity (RH, black line) in (c) on February 4–14.